Hydrogen Oxidation Reaction on Pt in Acidic Media: Adsorption Isotherm and Activation Free Energies

ARTICLE *in* THE JOURNAL OF PHYSICAL CHEMISTRY C · JULY 2007

Impact Factor: 4.77 · DOI: 10.1021/jp073400i

Hydrogen Oxidation Reaction on Pt in Acidic Media: Adsorption Isotherm and Activation Free Energies

Jia. X. Wang,*,† Thomas E. Springer,‡ Ping Liu,† Minhua Shao,† and Radoslav R. Adzic†

Department of Chemistry, Brookhaven National Laboratory, Upton, New York 11973, and Los Alamos National Laboratory, Electronic and Electrochemical Materials and Devices Group, Los Alamos, New Mexico 87545

Received: May 3, 2007; In Final Form: June 7, 2007

We present a method for quantifying the kinetic current of the hydrogen oxidation reaction (HOR) on Pt in acidic media using the adsorption and activation free energies as the intrinsic kinetic parameters. Our approach involves deriving the HOR intermediate's adsorption isotherm based on the same dual-pathway reaction model as for the kinetic equation. Coupled with density functional theory calculations of the coverage- and site-dependent hydrogen dissociation free energies, we analyzed the adsorption isotherms for H on atop (H_{Atop}) sites and in hollow/bridge ($H_{H/B}$) sites obtained respectively from infrared spectroscopic and electrochemical measurements. Although the hydrogen dissociative adsorption energy is not site-sensitive on Pt, H_{Atop} has an order of magnitude lower coverage and higher activity than $H_{H/B}$. We attributed this distinction to their different entropies; $H_{H/B}$ is less accessible to water than H_{Atop}, and the formation of a hydrogen bond is essential in the oxidative generation of H_3O^+. Using volcano plots, we illustrated possible ways that the exchange current may vary with the adsorption free energy and discussed the factors that contributed to the exceptionally high activity of Pt for the HOR.

1. Introduction

Growing interest in using hydrogen as a renewable fuel to resolve global energy concerns, climate change, and air quality has enhanced efforts to better understand the electrocatalytic behavior of platinum in the anodic hydrogen oxidation reaction (HOR)[1,2] and in the cathodic oxygen reduction reaction[3] in proton-exchange membrane fuel cells. These two widely studied reactions are considered the archetypal processes in electrocatalysis;[4−6] in both cases, the adsorption of the reaction intermediates is pivotal in determining the reaction rates. However, the relationship between adsorption isotherms of reaction intermediates and kinetic currents remains elusive.

The high activity of Pt for the HOR was well-recognized but was not clearly quantified until recently, partly because the reaction current exceeds the mass transport limitation over a very small potential region in rotating disk electrode (RDE) measurements. Using microelectrodes, Chen and Kucernak[7] obtained HOR polarization curves on Pt over a 400 mV potential region with a mass-transport limiting current up to 1 A cm^{-2}, that is, a hundred times higher than that previously obtained. Analyzing these data and those from the RDE measurements[8] using the dual-pathway kinetic equation, we demonstrated that the exchange current is two orders of magnitude higher than previously thought and that the Tafel slope strongly depends on overpotential.[9] These new findings cannot be fully understood without a better understanding of H adsorption.

For hydrogen reactions on Pt, two types of H adatoms differing in adsorption sites and adsorption energies were recognized first, as underpotentially and overpotentially deposited hydrogen, that is, H_{UPD} and H_{OPD} (see, e.g., refs 10 and 11). Infrared (IR) spectroscopy recently confirmed that the active intermediate for the HOR is adsorbed at atop sites,[12] as found earlier for the hydrogen evolution reaction[13,14] In contrast, the H_{UPD} apparently resides in hollow/bridge sites, embedded in the Pt surface's lattice, as inferred from IR and ultraviolet−visible reflectance measurements.[10] Furthermore, Protopopoff and Marcus found that hydrogen still is evolved even when manifold sites are completely blocked by chemisorbed S, and thus, they concluded that H_{UPD} is not a precursor for hydrogen evolution and oxidation.[15] Questions remain about the differences in the reaction activities of the two species, on how to describe their adsorption isotherms, and the effect of coexisting H_{UPD} on HOR kinetics.

We answered these questions in the present study by determining the free energies of adsorption and activations using an integrated approach combining density functional theory (DFT) calculations and experimental measurements. The usefulness of rigorously derived adsorption isotherms was demonstrated by their close agreement with measured adsorption isotherms for both active and inactive H adatoms, which is significant because the intermediate's coverage is not always measurable, and thus, unambiguous proof is important for establishing the concepts and methods we developed here.

The volcano-shaped curves in $\log(j_0)$ versus ΔG^0_{ad} plots have been widely used to explain trends of electrocatalytic activity of different metals and metal alloys.[16,17] In particular, Parsons[18] noted that the exchange current for the hydrogen evolution reaction passes through a maximum at zero adsorption free energy; later, DFT-calculated free energies afforded semiquantitative support.[19−21] Conway and Jerkiewicz[11] considered the possible positions for the H_{UPD} and H_{OPD} on a volcano curve. Here, we discuss our findings, shown in $\log(j_0)$ versus ΔG^0_{ad} plots for the two reaction pathways on two types of surface sites, and identify the factors contributing to the high activity of Pt for the HOR.

* To whom correspondence should be addressed. E-mail: jia@bnl.gov. Phone: +1-631-344-2515. Fax: +1-631-344-5815.
† Brookhaven National Laboratory.
‡ Los Alamos National Laboratory.

10.1021/jp073400i CCC: $37.00
Published on Web 07/27/2007

2. Kinetic Equation and Adsorption Isotherm

The detailed derivation presented below is based on the well-established kinetic model using commonly applied assumptions. Our major points are to introduce the concept of a reference prefactor, illustrate the relationship between activation and adsorption free energies, and derive the adsorption isotherm and kinetic equation using the same set of free energies as their intrinsic parameters.

On the basis of the Tafel−Heyrovsky−Volmer mechanism,[22−24] there are three elementary reaction steps for the $H_2 \leftrightarrows 2H^+ + 2e^-$ reaction on Pt catalysts:

$$H_2 \leftrightarrows 2H_{ad} \qquad \text{dissociative adsorption (DA)} \qquad (1)$$

$$H_2 \leftrightarrows H_{ad} + H^+ + e^- \qquad \text{oxidative adsorption (OA)} \qquad (2)$$

$$H_{ad} \leftrightarrows H^+ + e^- \qquad \text{oxidative desorption (OD)} \qquad (3)$$

The DA and OA reactions entail the atomic adsorption of hydrogen, while the OD reaction causes desorption of this reaction intermediate. One electron oxidation occurs in the OA and OD reactions, and hence, their reaction rates increase with increasing overpotential. We use these descriptive names to highlight the key feature of the elementary reactions in relation to their kinetic expressions. Conventionally, their net rates are expressed as the difference between those of the forward and those of the backward reactions:

$$\nu_{DA} = k_{DA} c_{H_2} (1-\theta)^2 - k_{-DA}\theta^2 \qquad (4)$$

$$\nu_{OA} = k_{OA} c_{H_2} e^{E/2kT}(1-\theta) - k_{-OA} c_{H^+} e^{-E/2kT}\theta \qquad (5)$$

$$\nu_{OD} = k_{OD} e^{E/2kT}\theta - k_{-OD} c_{H^+} e^{-E/2kT}(1-\theta) \qquad (6)$$

where k_i are the rate constants for the elementary reactions, and θ is the coverage for the active reaction intermediate, H_{HOR}. We assumed that the electron-transfer coefficient is 0.5 and used meV as the energy unit; namely, $kT = 25.7$ meV for $T = 298$ K, where the Boltzmann constant, $k = 0.08617$ meV K^{-1}.

Since we can assess the potential and free energies only relatively, the referencing points must be clarified. By definition, the net current is zero at the reversible potential, E^0. Thus, the exchange rate constants are defined as

$$\nu^0_{DA} = k_{DA} c_{H_2} (1-\theta^0)^2 = k_{-DA}(\theta^0)^2 \qquad (7)$$

$$\nu^0_{OA} = k_{OA} c_{H_2} e^{E^0/2kT}(1-\theta^0) = k_{-OA} c_{H^+} e^{-E^0/2kT}\theta^0 \qquad (8)$$

$$\nu^0_{OD} = k_{OD} e^{E^0/2kT}\theta^0 = k_{-OD} c_{H^+} e^{-E^0/2kT}(1-\theta^0) \qquad (9)$$

wherein the superscript "0" represents the zero overpotential, $\eta = E - E^0 = 0$. The H_2 and H^+ concentrations, c_{H_2} and c_{H^+}, are treated as potential-independent constants because here we consider only kinetic current; elsewhere, we discussed the treatment for the current measured under the mass-transport limitation.[9] The Nernst equation describes the dependence of E^0 on concentrations and temperature; in kinetic studies, we consider the potential-dependent current at constant concentrations and temperature. Thus, the reversible potential affords a convenient reference; that is, let $e^{-E^0/2kT} = 1$. Since all three reactions are at equilibrium, the standard adsorption free energy for $^1/_2H_2 \rightarrow H_{ad}$ at $\eta = 0$, ΔG^0_{ad}, is found by rearranging eqs 7−9

$$e^{-\Delta G^0_{ad}/kT} = \frac{\theta^0}{1-\theta^0} = \left[\frac{k_{DA} c_{H_2}}{k_{-DA}}\right]^{1/2} = \frac{k_{OA} c_{H_2}}{k_{-OA} c_{H^+}} = \frac{k_{-OD} c_{H^+}}{k_{OD} c_{H_2}} \qquad (10)$$

These relationships show that three pairs of forward and backward reaction-rate constants are correlated through a common adsorption free energy. Therefore, four independent parameters, rather than six, determine the reaction's kinetics.

The current density is directly proportional to the sum of the reaction rates for the two single electron-transfer reactions, ν_{OA} and ν_{OD}, and, under steady-state conditions, $d\theta/dt = 2\nu_{DA} + \nu_{OA} - \nu_{OD} = 0$; that is, $\nu_{OD} = 2\nu_{DA} + \nu_{OA}$. Thus, the currents of any two elementary reactions can express kinetic current wherein $j_i \equiv 2F\nu_i$

$$j_k = F(\nu_{OA} + \nu_{OD}) = 2F(\nu_{DA} + \nu_{OA}) = 2F(\nu_{OD} - \nu_{DA}) = (j_{OA} + j_{OD})/2 = j_{DA} + j_{OA} = j_{OD} - j_{DA} \qquad (11)$$

The reaction rate of the DA is obtained by dividing the three parts of eq 4 by their respective exchange rates in eq 7

$$\frac{\nu_{DA}}{\nu^0_{DA}} = \left(\frac{1-\theta}{1-\theta^0}\right)^2 - \left(\frac{\theta}{\theta^0}\right)^2 \qquad (12)$$

Rearranging eq 12 and noting that $j_{DA} = 2F\nu_{DA}$, we find the kinetic current for this reaction is

$$j_{DA} = \frac{2F\nu^0_{DA}}{(1-\theta^0)^2}\left[(1-\theta)^2 - \left(\frac{1-\theta^0}{\theta^0}\right)^2\theta^2\right] \qquad (13)$$

Similarly, we obtained the kinetic current for the OA and OD respectively from eqs 5 and 8 and eqs 6 and 9,

$$j_{OA} = \frac{2F\nu^0_{OA}}{(1-\theta^0)}\left[e^{\eta/2kT}(1-\theta) - e^{-\eta/2kT}\left(\frac{1-\theta^0}{\theta^0}\right)\theta\right] \qquad (14)$$

$$j_{OD} = \frac{2F\nu^0_{OD}}{\theta^0}\left[e^{\eta/2kT}\theta - e^{-\eta/2kT}\left(\frac{\theta^0}{1-\theta^0}\right)(1-\theta)\right] \qquad (15)$$

Then, the intrinsic exchange currents were defined and correlated with the reaction rate constants, k_i, based on eqs 7−9

$$j^0_{DA} \equiv 2F\nu^0_{DA}/(1-\theta^0)^2 = 2Fk_{DA}c_{H_2} = j^*_{DA} e^{-\Delta H^{*0}_{DA}/kT} = j^* e^{-\Delta G^{*0}_{DA}/kT} \qquad (16)$$

$$j^0_{OA} \equiv 2F\nu^0_{OA}/(1-\theta^0) = 2Fk_{OA}c_{H_2} = j^*_{OA} e^{-\Delta H^{*0}_{OA}/kT} = j^* e^{-\Delta G^{*0}_{OA}/kT} \qquad (17)$$

$$j^0_{OD} \equiv 2F\nu^0_{OD}/\theta^0 = 2Fk_{OD} = j^*_{OD} e^{-\Delta H^{*0}_{OD}/kT} = j^* e^{-\Delta G^{*0}_{OD}/kT} \qquad (18)$$

The word "intrinsic" means that the thus defined exchange currents are coverage-independent. They can be rewritten in the format of the Arrhenius equation with j^*_i being the pre-exponential factor representing the frequency factor for each reaction in units of current density. In terms of free energy, we note that $e^{-\Delta G/kT} = e^{-\Delta H/kT} e^{\Delta S/k}$, and thus, the frequency factor is related to entropy; that is, $j^*_i = j^* e^{\Delta S^{*0}_i/kT}$, where j^* acts as a scaling or converting factor allowing us to express the differ-

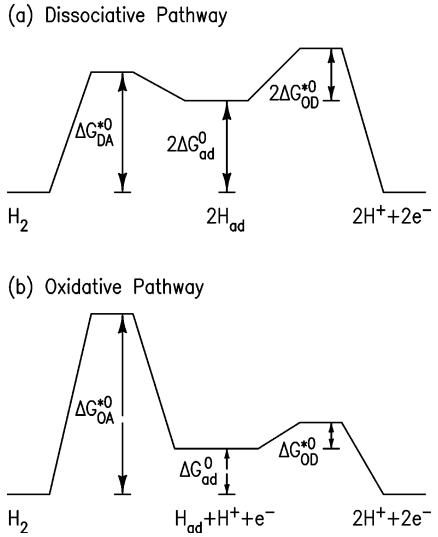

Figure 1. Free energies of activation and adsorption defined (a) for the dissociative, and (b) the oxidative pathways of the HOR on Pt at the reversible potential.

ences in intrinsic exchange currents by the corresponding activation free energies. Comparing this above-defined relationship,

$$\Delta G_i^{*0} = \Delta H_i^{*0} - T\Delta S_i^{*0} = \Delta H_i^{*0} - kT\ln(j_i^*) + kT\ln(j^*) \quad (19)$$

to that used in theoretical calculations,

$$\Delta G_i^{*0} = \Delta E_i^{*0} - T\Delta S_i^{*0} + \Delta E_{ZPE} \quad (20)$$

we obtain $\Delta H_i^{*0} = \Delta E_i^{*0}$ since $P\Delta V$ is negligible, $\Delta S_i^{*0} = k\ln(j_i^*)$, and $kT\ln(j^*) = \Delta E_{ZPE}$, where ZPE represents zero point energy.[25] Analogous to the reference electrode for potential, we term j^* the reference prefactor.

Combining eqs 13−15 with eqs 16−18 and eq 10 yields expressions for kinetic currents using the activation free energies for the forward reactions and the adsorption free energy as the adjustable parameters,

$$j_{DA} = j^* e^{-\Delta G^{*0}_{DA}/kT}[(1-\theta)^2 - e^{2\Delta G^0_{ad}/kT}\theta^2] \quad (21)$$

$$j_{OA} = j^* e^{-\Delta G^{*0}_{OA}/kT}[e^{\eta/2kT}(1-\theta) - e^{\Delta G^0_{ad}/kT} e^{-\eta/2kT}\theta] \quad (22)$$

$$j_{OD} = j^* e^{-\Delta G^{*0}_{OD}/kT}[e^{\eta/2kT}\theta - e^{-\Delta G^0_{ad}/kT} e^{-\eta/2kT}(1-\theta)] \quad (23)$$

Figure 1 illustrates how the four independent free energies, three for activation barriers and one for the adsorption of the reaction intermediate, determine the free energy diagrams for the two reaction pathways.

To derive the corresponding adsorption isotherm for the reaction intermediate, we introduce another expression for eqs 21−23, in which the forward- and backward-reaction currents are formulated using their corresponding activation free energies,

$$j_{DA} = j^* e^{-\Delta G^*_{DA}/kT}(1-\theta)^2 - j^* e^{-\Delta G^*_{-DA}/kT}\theta^2 \quad (24)$$

$$j_{OA} = j^* e^{-\Delta G^*_{OA}/kT}(1-\theta) - j^* e^{-\Delta G^*_{-OA}/kT}\theta \quad (25)$$

$$j_{OD} = j^* e^{-\Delta G^*_{OD}/kT}\theta - j^* e^{-\Delta G^*_{-OD}/kT}(1-\theta) \quad (26)$$

where

$$\Delta G^*_{DA} = \Delta G^{*0}_{DA} \quad (27)$$

$$\Delta G^*_{-DA} = \Delta G^{*0}_{DA} - 2\Delta G^0_{ad} \quad (28)$$

$$\Delta G^*_{OA} = \Delta G^{*0}_{OA} - 0.5\,e\eta \quad (29)$$

$$\Delta G^*_{-OA} = \Delta G^{*0}_{OA} - \Delta G^0_{ad} + 0.5\,e\eta \quad (30)$$

$$\Delta G^*_{OD} = \Delta G^{*0}_{OD} - 0.5\,e\eta \quad (31)$$

$$\Delta G^*_{-OD} = \Delta G^{*0}_{OD} + \Delta G^0_{ad} + 0.5\,e\eta \quad (32)$$

Equations 27−32 can be modified to treat the coverage-dependent lateral repulsion as a potential-dependent variable. The results obtained by using this more sophisticated model are given in Supporting Information.

To find the adsorption isotherm, $\theta(\eta)$, we note that $\nu_i = j_i/2F$ and let $g_i = e^{-\Delta G_i^*/kT}$. Combining the steady-state equation, $d\theta/dt = 2\nu_{DA} + \nu_{OA} - \nu_{OD} = 0$, with eqs 24−26 leads to

$$2g_{DA}(1-\theta)^2 - 2g_{-DA}\theta^2 + g_{OA}(1-\theta) - g_{-OA}\theta = g_{OD}\theta - g_{-OD}(1-\theta) \quad (33)$$

Equation 33 can be rearranged into a quadratic equation, $A\theta^2 + B\theta + C = 0$, where

$$A = 2g_{DA} - 2g_{-DA} \quad (34)$$

$$B = -4g_{DA} - g_{OA} - g_{-OA} - g_{OD} - g_{-OD} \quad (35)$$

$$C = 2g_{DA} + g_{OA} + g_{-OD} \quad (36)$$

whose solution, after taking the correct root, becomes

$$\theta = \frac{-B - \sqrt{B^2 - 4AC}}{2A}, \quad A \neq 0; \qquad \theta = -\frac{C}{B}, \quad A = 0 \quad (37)$$

For fitting the polarization curves, we use eq 38 to calculate the measured current,

$$j = \frac{j_k}{1 + j_f/j_L} \quad (38)$$

where j_L is the mass-transport-limiting current, and j_f is the partial kinetic current for the forward reactions. For example, $j_f = j_{+DA} + j_{+OA}$ when $j_k = j_{DA} + j_{OA}$ is chosen from the three equivalent expressions in eq 11. Then, the exchange current, as defined by the amplitude of the kinetic current at zero overpotential, can be found

$$j_0 \equiv j_f(\eta = 0) = j^0_{DA}(1-\theta^0)^2 + j^0_{OA}(1-\theta^0) \quad (39)$$

In summary, this derivation demonstrated that we generated an exact solution for the adsorption isotherm of the reaction intermediate without introducing new parameters independent of those already in the equations for kinetic currents. That is, the kinetic current, $j_k(\eta) = f(\Delta G^{*0}_{DA}, \Delta G^{*0}_{OA}, \Delta G^{*0}_{OD}, \Delta G^0_{ad}, j^*, \theta)$, can be obtained using eq 11 and any two of eqs 21−23, in

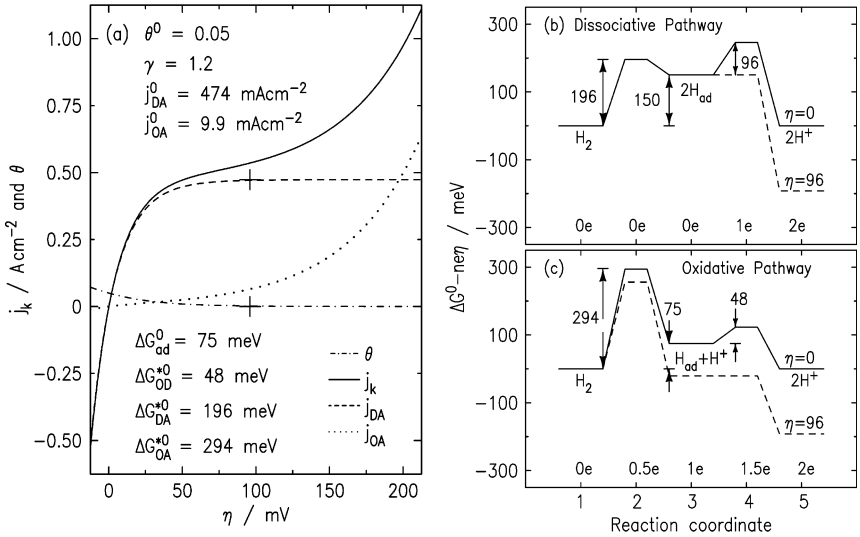

Figure 2. (a) HOR kinetic current (j_k) and its two components: the partial kinetic currents from the DA (j_{DA}) and OA (j_{OA}) pathways as a function of overpotential, and the intermediate's adsorption isotherm (θ) were generated using the dual-pathway kinetic equation with the parameters given in the upper part of the figure. The corresponding free energies (with $j^* = 1000$ A cm^{-2}) are given in the lower part. (b,c) Free-energy diagrams constructed using the free energies given in (a) at $\eta = 0$ (solid lines) and $\eta = 96$ mV (dashed lines).

which the adsorption isotherm, $\theta(\eta) = f(\Delta G^{*0}_{DA}, \Delta G^{*0}_{OA}, \Delta G^{*0}_{OD}, \Delta G^{0}_{ad})$, is determined by eqs 27−37.

3. The Reference Prefactor and Free Energy Diagrams

We previously analyzed the polarization curves measured under different mass-transport conditions using a simplified dual-pathway kinetic equation with j^0_{DA}, j^0_{OA}, θ^0, and γ as the adjustable kinetic parameters,

$$j_k = j^0_{DA}[(1-\theta)^2 - (1-\theta^0)^2(\theta/\theta^0)^2] + j^0_{OA}[(1-\theta)\, e^{\eta/2kT} - (1-\theta^0)(\theta/\theta^0)\, e^{-\eta/2kT}] \quad (40)$$

and employing an approximate expression for the adsorption isotherm (see the appendix in ref 9),

$$\theta = \frac{\theta^0 e^{-\eta/\gamma kT}}{1-\theta^0+\theta^0 e^{-\eta/\gamma kT}} \quad (41)$$

where γ is the adsorption-range constant determined approximately by eq 42,

$$\gamma \approx \frac{4j^0_{DA}(1-\theta^0)^2 + j^0_{OA}(1-\theta^0) + j^0_{OD}\theta^0}{j^0_{OD}\theta^0 - j^0_{OA}(1-\theta^0)} \quad (42)$$

Figure 2a shows the kinetic currents and adsorption isotherm calculated with the fitted parameters listed in its upper sector. The exchange current calculated from eq 39 is 437 mA cm^{-2}, that is, two orders of magnitude higher than that from the Butler−Volmer equation. We earlier discussed this discrepancy in detail.[9] These curves are reproduced using the fitted free energies with $j^* = 1000$ A cm^{-2}, as shown in the lower part of the figure. Next, we explain how they were determined.

The free energy of adsorption has a one-to-one correlation with the equilibrium coverage, given by $\Delta G^0_{ad} = kT \ln[(1-\theta^0)/\theta^0]$. By fitting the polarization curves measured with microelectrodes, we found $0 \le \theta^0 \le 0.3$ monolayer, while Quaino et al. reported $\theta^0 \approx 10^{-7}$ from these same data.[26] To reduce uncertainty, we further analyzed the polarization curves measured with a smooth rotating electrode (low mass-transport rate, high sensitivity to θ^0). The best fit yielded $\theta^0 = 0.05$ corresponding to $\Delta G^0_{ad} = 75$ meV, with the low and high error bars at 56 meV ($\theta^0 = 0.1$), and 118 meV ($\theta^0 = 0.01$), respectively.

To select a suitable value for the reference prefactor, we assumed that the activation free energy for the OD corresponds to twice the half-coverage potential, which is determined from eq 41, that is, $\eta_{1/2} = \gamma kT \ln[(2-\theta^0)/(1-\theta^0)]$ and $\Delta G^{*0}_{OD} = 2e(\eta_{1/2}) = 44$ meV, using the experimentally determined parameters, $\gamma = 1.2$ and $\theta^0 = 0.05$. We obtained good correspondence to the data and identical kinetic current curves when fitting with free energies using $200 < j^* < 5000$ A cm^{-2}. We chose $j^* = 1000$ A cm^{-2} because it yields $\Delta G^{*0}_{OD} = 48$ meV, close to the value found by $2e(\eta_{1/2})$. A difference factor of 200/1000 = 1/5 or 5000/1000 = 5 in j^* shifts $kT \ln(1/5) = -41$ meV or $kT \ln(5) = 41$ meV for all three activation free energies. This uncertainty originates from the inability to evaluate the exact contributions from entropy and enthalpy from a reaction rate without measuring its temperature dependence.

From quantum mechanical calculations, Cai and Anderson obtained 76 meV for the activation energy of the OA reaction,[27] considerably smaller than our 294 meV. This is understandable since our value for free energy contains the contribution from entropy, and the effect of lateral repulsion from the H_{UPD} is not included in their calculations.

Figure 2b,c illustrates the corresponding free energy diagrams for the two reaction pathways. At $\eta = 0$, the free energies of the reactant, H_2, equal that of the products, $2H^+ + 2e^-$. Between them, we include one reaction intermediate and two transition states. The oxidative pathway has a half-electron transfer at each step with one H adatom at the middle, so that the free energy curve (solid line) is constructed straightforwardly using the values from Figure 2a. In contrast, electron transfer is not involved in the dissociative adsorption of H_2, and the reaction yields two H adatoms. Therefore, the free energies of adsorption and activation for the OD in the DA pathway are double those in the OA pathway.

As the overpotential increases, the free energies determined by $\Delta G^0 - ne\eta$ fall. The dashed lines in Figure 2b,c illustrate that, at $\eta = 96$ mV, twice the value of ΔG^0_{OD} the energy barrier for the OD vanishes, where the coverage of the reaction intermediate becomes negligible, and the current for the

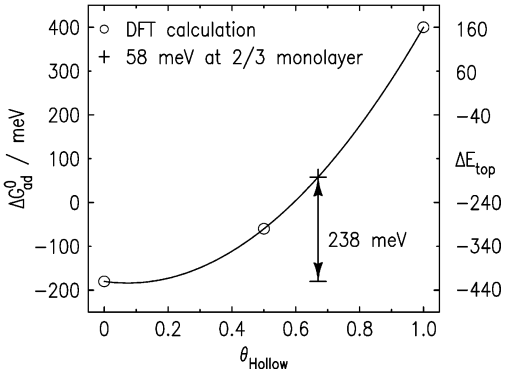

Figure 3. Calculated H adsorption energy at atop sites on Pt(111), right scale, and the corresponding free energy of H adsorption, ΔG^0_{ad}, as a function of the coverage for pre-adsorbed H at hollow sites (circles). The solid line is the quadratic fit to the calculated values.

dissociative pathway reaches its maximum, as marked by the plus sign in Figure 2a. This relationship illustrates the importance of a low ΔG^0_{OD} for high activity. From the free-energy diagram in Figure 2b, we find that the activation barrier for the backward reaction of DA, $\Delta G^{*0}_{-DA} = \Delta G^{*0}_{DA} - \Delta G^0_{ad} = 196 - 150 = 46$ meV, is comparable to ΔG^{*0}_{OD}. Therefore, the competition between OD and backward DA determines the activity at low overpotentials. A high backward reaction rate also closely ties the kinetic current to the intermediate's coverage, even though the site-blocking effect is very small for coverage below 0.05.

4. DFT Calculations

To evaluate the adsorption free energy as a function of coverage and on different sites, we undertook DFT calculations to assess the dissociative adsorption of hydrogen on a Pt(111) surface with pre-adsorbed hydrogen adatoms in the face centered cubic (fcc) hollow sites with zero, half, and unity coverage using a 2×1 supercell.[28] Experimentally, the H_{UPD} was found mainly in hollow or bridge sites,[10] its coverage increasing continuously with decreasing potential to a saturated value of a 2/3 monolayer.[29] We chose a commensurate structure for the pre-adsorbed H_{UPD} in hollow sites to have a small supercell, thereby reducing computational effort. For an H adatom at atop sites, the calculated adsorption energies, ΔE_{Atop}, are 420, 300, and 160 meV with pre-adsorbed H being zero, a half, and a full monolayer, respectively. Figure 3 plots them (as circles) using the right-side axis, while the left-side axis shows the corresponding values for ΔG^0_{ad} obtained by a shift of 240 meV to account both for the zero-point energy correction and for the entropic contribution to free energy.[25] The solid line is the fit to a quadratic equation,

$$\Delta G_{ad} = a\theta_{UPD} + b\theta_{UPD}^2 = -100\theta_{UPD} + 680\theta_{UPD}^2 \qquad (43)$$

which yields $\Delta G^0_{ad} = 58$ meV at $\theta_{UPD} = 2/3$ monolayer, agreeing reasonably with 75 meV from our kinetic analysis. The energy difference is 238 meV between zero and the saturated coverage of 0.67 at the reversible potential, corresponding to a g factor $238/0.67/kT = 14$. Analyzing temperature-dependent voltammetry curves, Zolfaghari and Jerkiewicz[30] obtained a g factor of 11, while Adzic et al. found a value of 17 using the Temkin adsorption isotherm.[31]

Our DFT calculations showed that adsorption at atop sites is 30 meV or approximately 10% stronger than that in hollow sites for $\theta_{UPD} = 0.5$. Since the DFT calculations have 0.1 eV uncertainties, the hydrogen adsorption energy on Pt is considered site-insensitive. This is an important, distinctive property of Pt, as other DFT calculations found that H adsorption on atop sites is approximately 4% higher than that in hollow and bridge sites for Pt but approximately 83% and 97% lower for Ni and Pd, respectively.[32] Furthermore, the diffusion barrier from an atop to an fcc site is only about 10 meV.[33] Therefore, the DA reaction rate should be essentially the same for all surface sites, either through direct adsorption or via atop-site adsorption followed by nearly barrier-less diffusion.

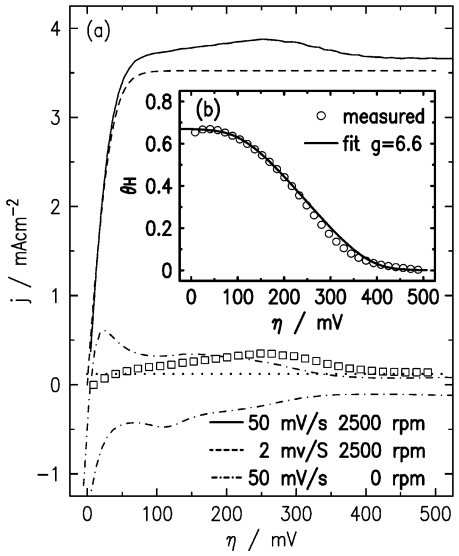

Figure 4. (a) HOR polarization curves measured on a Pt/C (20 wt % Pt on carbon support from E-TEK) thin film rotating disk electrode at 23 °C in hydrogen-saturated 0.1 M $HClO_4$ solution at 50 mV/s (dashed line) and 2 mV/s (solid line). (b) Coverage of adsorbed H under HOR condition.

Conversely, the OD and OA reaction rates may differ at different sites because atop sites are more accessible to water than bridge/hollow ones, and hydrogen bonding with water is important in the oxidative formation of H_3O^+ as illustrated by molecular dynamic simulation.[34] For the ORR, the prefactor for processes involving hydrogenation was correspondingly smaller than that for oxygen dissociation by the equivalent of an additional 130 meV activation barrier.[35] Although H_3O^+ is the product, not the reactant, in the HOR, water can be considered as the reactant in forming H_3O^+; thus, its formation is sensitive to the accessibility of water. Therefore, we expect entropies for the OD and OA reactions to be different for atop and bridge/hollow sites which, in turn, can cause differences in adsorption isotherms and activities for the HOR. To verify this idea, we determined, by in situ voltammetry, the total coverage of H under a steady-state condition and measured its atop-site coverage by IR spectroscopy.

5. Electrochemical and IR Measurements of H Adsorption

Figure 4 shows the polarization and voltammetry curves measured on a Pt nanoparticle thin-film electrode in 0.1 M $HClO_4$ solution and the deduced H adsorption isotherm; the features are typical for Pt particles with nano- to micrometer diameters. In the absence of hydrogen, the θ_{UPD} is often obtained by integrating voltammetry curves after subtracting a constant current for double-layer charging. A complication arises near the reversible potential because hydrogen is evolved below 50 mV, and the product is oxidized in the positive potential sweep (marked by the dotted-dashed line). To separate the HOR current

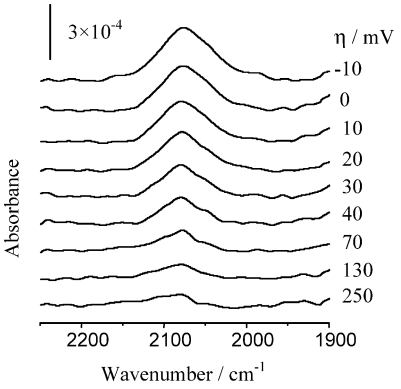

Figure 5. Infrared spectra of H adatoms measured on a Pt thin-film electrode in 0.1 M $HClO_4$ solution saturated with pure hydrogen (1 atm pressure) at room temperature (23 °C). The potential was measured against a Ag/AgCl electrode and converted to the HOR overpotential, η, using the measured open-circuit potential. The reference spectrum was collected at 0.87 V in the same solution.

from that for desorption of the H_{UPD}, we measured the polarization curves at 50 and 2 mV/s with 2500 rpm rotating rate. Since H adsorption/desorption is highly reversible, we assumed that the HOR currents are the same under both conditions and that the current for desorption of H at 2 mV/s is negligible compared with that at 50 mV/s. Thus, the difference between the two curves (squares) is attributed to H desorption plus the difference in double-layer charging at two sweep rates; the latter is assumed to be a potential-independent constant (dotted line). This current curve (squares) peaks at a more positive potential (about 60 mV) than that without hydrogen (dotted-dashed line), revealing the effect of H concentration on the hydrogen-adsorption isotherm. After subtracting a constant double-layer charging current (dotted line), the current corresponding to H desorption was integrated and converted to coverage with the maximum value being a 2/3 monolayer (circles in Figure 4b).

Fitting with the Frumkin isotherm (solid line) yielded a g factor of 6.6 for lateral repulsion. However, this common approach is inappropriate for kinetic analysis because all three elementary reactions affect the H adsorption isotherm in the presence of hydrogen, while the Frumkin and Langmuir isotherms are based on the equilibrium of a single reaction. We next describe our analysis using the intrinsic adsorption isotherm derived in section 2.

Surface-enhanced infrared absorption spectroscopy measurements were carried out with a Pt thin film chemically deposited on a hemispherical Si crystal in hydrogen-saturated 0.1 M $HClO_4$; experimental details were given previously.[36] Figure 5 shows the spectra at different overpotentials using as a reference that collected at 0.87 V. To minimize possible CO contamination,[12] the potential was held at 0.87 V for 10 s before stepping to that required for each measurement. Spectra are given in absorbance, defined as $A = -\log(R/R_0)$, where R and R_0 represent the reflected IR intensities corresponding respectively to the sample and reference spectra. The IR beam was unpolarized, spectral resolution was set to 8 cm^{-1} per point, and 512 interferograms were added for every spectrum.

The peak centered near 2090 cm^{-1} was attributed to the atop-site H, the known active intermediate for the HOR.[12] Without optimizing the Pt thin film, our band intensities are weaker than those reported by Kunimatsu et al.;[12] nevertheless, the potential dependence of integrated band intensities agree well with their results. The adsorption isotherm for the H_{Atop} in Figure 6a was obtained by normalizing the IR band intensities to 0.05 for η = 0, that is, the equilibrium coverage we determined from kinetic analysis.[9] Since the θ_{Atop} is much smaller than the total H coverage measured electrochemically, we assume that the latter approximately represents the coverage for H in hollow/bridge sites ($H_{H/B}$).

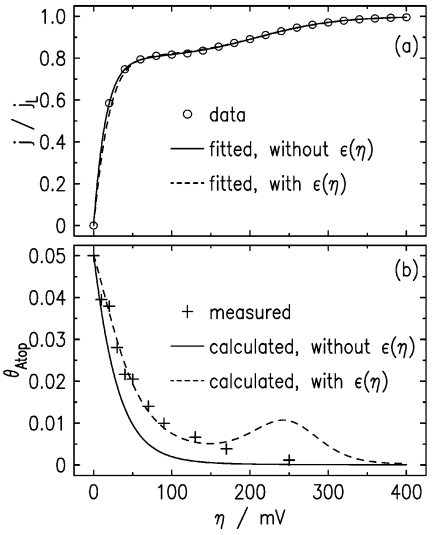

Figure 6. (a) Best fits to a normalized ($j_L = 120$ mA cm^{-2}) polarization curve (circles) for the HOR (1 atm pure hydrogen) on a Pt microelectrode in 0.1 M H_2SO_4 solutions at 23 °C obtained by Chen and Kucernak.[7] (b) Adsorption isotherm obtained from IR measurements with the calculated curves using the parameters obtained from fits in (a).

6. Site-Dependent Adsorption and Activity

Figure 6 shows the IR-measured adsorption isotherm (plus signs) and a typical microelectrode polarization curve from Chen and Kucernak.[7] The solid and dashed lines were calculated with the parameters obtained from the best fits to the polarization curve using the models without and with potential-dependent lateral repulsion, $\epsilon(\eta)$, respectively. The values of fitted free energies for the former are the same as those in Figure 2a. For the latter, the coverage-dependent lateral repulsion is treated as a potential-dependent variable using the DFT-calculated coverage dependence and electrochemically measured adsorption isotherm; full details appear in Supporting Information. Our conclusions are (1) the more sophisticated model has marginal impact for the kinetic current; that is, both models yield good fits to the data and nearly identical kinetic currents (Figure 6a), and (2) the corresponding adsorption isotherms are largely consistent with the measured adsorption isotherm for the H_{Atop} (Figure 6b).

Figure 7 plots the adsorption isotherms for the H_{Atop} and $H_{H/B}$ and the corresponding kinetic currents. The data for the $H_{H/B}$ were obtained from the electrochemical measurements and fitted using eqs 27−37 with ΔG^0_{DA} fixed at 196 meV. This choice rested on our DFT calculations showing hydrogen dissociation energy is site-insensitive. The adsorption free energy of −18 meV was determined by $\Delta G^0_{ad} = kT \ln[(1 - \theta^0)/\theta^0]$, with θ^0 being 0.67. The activation free energies for the two reactions involving the oxidative formation of H_3O^+, ΔG^{*0}_{OA} and ΔG^{*0}_{OD}, were considered site-sensitive; hence, they were varied during fitting.

The values from the fits listed in Figure 7b show that ΔG^{*0}_{OD} and ΔG^{*0}_{DA} are significantly higher for the $H_{H/B}$ than for the H_{Atop}. We attributed the higher activation free energies to the lesser chance of H forming hydrogen bonds with water in

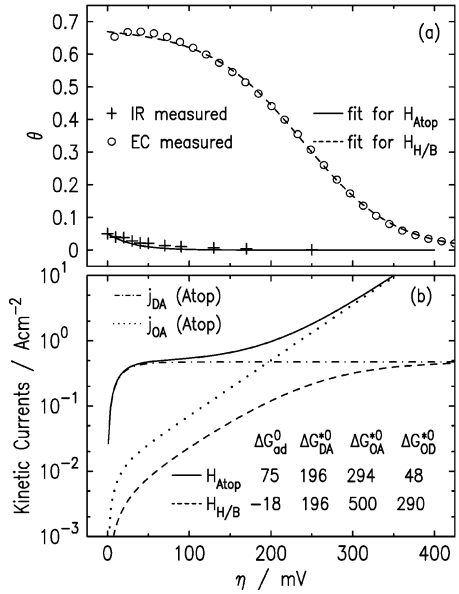

Figure 7. (a) Adsorption isotherms obtained from IR and electrochemical measurements with the fits for H adsorbed on atop sites and in hollow/bridge sites, respectively. (b) Kinetic currents on logarithmic scale calculated using fitted free energies (meV).

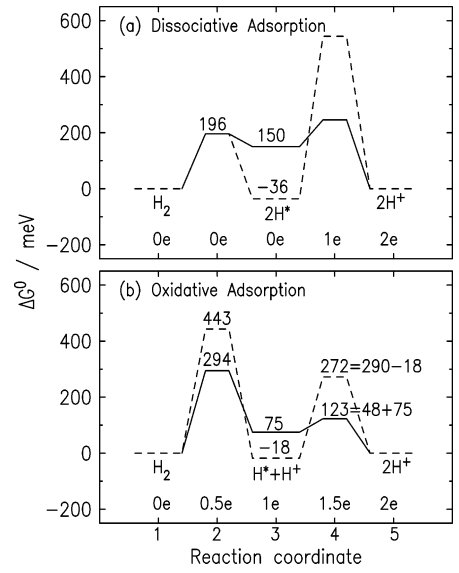

Figure 8. Free-energy diagrams for HOR on Pt constructed for H adsorption on atop (solid lines) and in hollow/bridge (dashed lines) sites using the free energies determined from analyzing the polarization curves and the electrochemically measured adsorption isotherm.

hollow/bridge sites than at atop sites. This entropic difference should be considerable because the H atom is much smaller than the Pt atom, and thus, the H adatoms are embedded in the substrate lattice if they are not at atop sites. From temperature-dependent measurements, the entropy for the H_{UPD} (i.e., the $H_{H/B}$) was -63 J mol^{-1} K^{-1} at 2/3 coverage.[30] The corresponding $-T\Delta S$ value for $T = 298$ K is 194 meV, comparable to the difference in ΔG^{*0}_{OD} between the $H_{H/B}$ and the H_{Atop}, 195 meV.

Using the determined free energies, we depict the calculated kinetic currents for these two types of sites in Figure 7b. Their order of magnitude difference illustrates the role of adsorption isotherm in determining kinetic behavior. The curves in Figure 7b are nonlinear indicating that the Tafel slope varies with overpotential over a wide potential region. The "normal" value for the DA pathway approaches infinity since its reaction rate is potential independent, while that for the OA pathway is $2.303kT/0.5 = 118$ mV/dec. These limiting values are reached for atop sites when the H_{Atop} nearly vanishes around 50 mV. The Tafel slope of the overall kinetic current continues to vary at higher overpotentials as the relative contribution from the two pathways changes with increasing potential. For hollow/bridge sites, the DA pathway dominates up to 300 mV, where the change of Tafel slope follows that in the adsorption isotherm for the $H_{H/B}$.

7. Exchange Current and Its Relationship with Adsorption Free Energy

Figure 8 summarizes the results from the dual pathway with two distinct surface sites; it reveals that ΔG^{*0}_{DA} is the same at atop and hollow/bridge sites while ΔG^{*0}_{OA} and ΔG^{*0}_{OD} are significantly lower for atop ones. Further, adsorption free energy differs considerably. Below, we discuss the correlation between free energies and electrocatalytic activities.

Exchange currents, often used to represent the activities of various metal and metal alloy surfaces for hydrogen evolution/oxidation reactions,[18,21,25,37,38] can be correlated with the adsorption free energy by combining eqs 39 and 10; that is,

$$j_0 = j^0_{DA}(1-\theta^0)^2 + j^0_{OA}(1-\theta^0) = \frac{j^* e^{-\Delta G^{*0}_{DA}/kT}}{(1+e^{-\Delta G^0_{ad}/kT})^2} + \frac{j^* e^{-\Delta G^{*0}_{OA}/kT}}{(1+e^{-\Delta G^0_{ad}/kT})} \equiv j_{0,DA} + j_{0,OA} \quad (44)$$

In logarithmic format,

$$\log(j_{0,DA}) = \log(j^*) - \Delta G^{*0'}_{DA}/(2.3kT) - 2\lambda\Delta G^0_{ad}/(2.3kT) - 2\log(1+e^{-\Delta G^0_{ad}/kT}) \quad (45)$$

$$\log(j_{0,OA}) = \log(j^*) - \Delta G^{*0'}_{OA}/(2.3kT) - \lambda\Delta G^0_{ad}/(2.3kT) - \log(1+e^{-\Delta G^0_{ad}/kT}) \quad (46)$$

Here, we assumed that the activation free energies linearly depend on the adsorption free energy, i.e., $\Delta G^{*0}_{DA} = \Delta G^{*0'}_{DA} + \lambda(2\Delta G^0_{ad})$ and $\Delta G^{*0}_{OA} = \Delta G^{*0'}_{OA} + \lambda\Delta G^0_{ad}$, where λ is the correlation coefficient for the effect of adsorption free energy on the activation free energies, and $\Delta G^{*0'}_{DA}$ and $\Delta G^{*0'}_{OA}$ are the activation free energies when $\Delta G^0_{ad} = 0$ or $\theta^0 = 0.5$.

Figure 9 depicts θ^0, $\log(j_{0,DA})$, and $\log(j_{0,OA})$ as a function of ΔG^0_{ad} calculated respectively with eqs 10, 45, and 46. The sum of the first two terms in eqs 45 and 46 determines the maximum exchange currents, which are approached with slightly positive ΔG^0_{ad} for $\lambda = 0$ (solid lines) or slightly negative ΔG^0_{ad} for $\lambda = 1$ (dotted lines). The curves become symmetric when $\lambda = 0.5$, with a smaller maximum value at $\Delta G^0_{ad} = 0$, where $\theta^0 = 0.5$. The inserts in Figure 9a illustrate the correlation between ΔG^{*0}_{DA} and ΔG^0_{ad} for $\lambda = 0.5$ and $\lambda = 0$.

Parsons[17] qualitatively described the symmetric curve with its maximum at $\Delta G^0_{ad} = 0$, wherein Δg^0 corresponds to ΔG^0_{ad}, while $\alpha = 0.5$ corresponds to $\lambda = 0.5$ in ours. When the difference in ΔE dominates, it is reasonable to choose $\alpha = 0.5$ by assuming that the shape of the energy curve is constant, thereby generating the volcano-type curve. This result is consistent with, but not equivalent to, the Sabatier principle stating that catalytic activity is optimal on a catalytic surface with intermediate binding energy for reactive intermediates.[39]

Because free energy encompasses enthalpy and entropy, the symmetry factor is not the only one determining the correlation coefficient; so, we define λ as an unrestricted constant, which

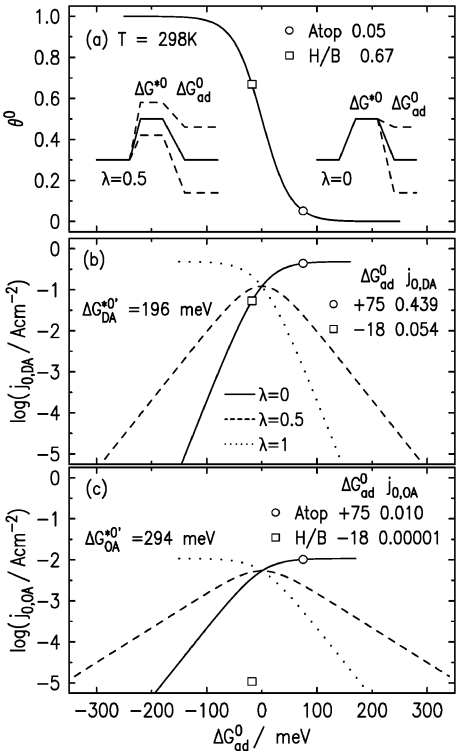

Figure 9. Equilibrium coverage (a) and exchange currents of two reaction pathways (b,c) as a function of the H adsorption free energy calculated using eqs 10, 45, and 46, respectively, with $j^* = 1000$ A cm^{-2} and $\lambda = 0$ (solid lines), $\lambda = 0.5$ (dashed lines), and $\lambda = 1$ (dotted lines). The inserts in (a) show the variance of activation barrier with adsorption free energy when $\lambda = 0$ and 0.5.

can, but not necessarily does, represent the symmetry factor. The case for the HOR on atop and in hollow/bridge Pt sites offers examples where λ can be zero, for example, the value for the ΔG^{*0}_{DA} remains constant for both even when their ΔG^0_{ad} differ (see Figure 8a) or where λ is negative, for example, ΔG^{*0}_{OA} is even higher for the $H_{H/B}$ than H_{Atop} while the former has a lower ΔG^0_{ad} than the latter (see Figure 8b). Therefore, the corresponding log($j_{0,DA}$) versus ΔG^0_{ad} data points are on the $\lambda = 0$ line in Figure 9b, while those for log($j_{0,OA}$) versus ΔG^0_{ad} cannot be connected by the lines in Figure 9c.

The fact that the exchange currents can overreach the maximum in the symmetric curve reminds us that the volcano curves are model-dependent, that is, incorporate assumptions correlating activation and adsorption free energies. The Sabatier principle holds independently of the models because it states the trend without specifying an explicit maximum activity and optimal adsorption energy. The real maximum value in the log(j_0) versus ΔG^0_{ad} plots is higher than the maximum of the volcano curve by 2log(2) and log(2) for the DA and OA reactions, respectively. The results for the HOR on different Pt sites demonstrate that these real maxima can be approached with a slightly positive ΔG^0_{ad}.

8. Conclusions

Using our rigorously derived adsorption isotherm and kinetic equation, we verified that the HOR on Pt in acidic media occurs via two reaction pathways and has two types of adsorption sites distinguishable by their free energies of adsorption and activation for elementary reactions. While the hydrogen dissociation energy on Pt is site-insensitive, the activation free energies for the OD and OA reactions, deduced from analyzing the IR measured and electrochemically measured adsorption isotherms, are significantly lower for atop sites than those for hollow/bridge sites. We attribute these differences to the difference in entropy because the $H_{H/B}$ is less accessible to water than the H_{Atop}, and hydrogen-bond formation is essential in the oxidative generation of H_3O^+.

The following factors contributed to the exceptional high activity of Pt for the HOR: (1) The low, site-insensitive dissociation barrier in the rate-determining step leading to a high adsorption rate on atop sites and negligible site blocking by the inactive H in hollow/bridge sites; (2) lateral repulsion from inactive $H_{H/B}$ ensuring a small equilibrium coverage for H on active atop sites, and thus, a high exchange current; and (3) a very low barrier for the oxidative desorption of the H_{Atop} so facilitating a rapid rise of the net reaction rate at low overpotentials.

The concepts and methods developed are applicable for other electrocatalytic reactions. For example, we introduced a reference prefactor, assigning it a value of 1000 A cm^{-2} that is suitable as a standard for comparing activation free energies, as is the normal hydrogen electrode for comparing potentials. We constructed free energy diagrams, including transition states, using them as a platform to directly compare and reconcile theoretical and experimental results. This integrated approach may well-resolve outstanding issues in other electrocatalyzed reactions

Acknowledgment. This work is supported by the U.S. Department of Energy, Divisions of Chemical and Material Sciences, under Contract No. DE-AC02-98CH1-886. We thank Dr. Marshall D. Newton for useful discussions.

List of Symbols

c (M or mol cm^{-3})	concentrations of reactants or products
E^0 (V)	reversible potential for HOR
j (A cm^{-2})	measured current density
j_{DA} , $j_{OA,}$, j_{OD} (A cm^{-2})	partial kinetic current densities of elementary reactions
j^0_{DA}, j^0_{OA}, j^0_{OD} (A cm^{-2})	intrinsic exchange current densities of elementary reactions
$j_{0,DA}$, $j_{0,OA}$ (A cm^{-2})	exchange current densities
j_0 (A cm^{-2})	exchange current density
j^* (A cm^{-2})	reference prefactor
j^*_i (A cm^{-2})	prefactor for elementary reactions i = DA, OA, OD
j_k (A cm^{-2})	total net kinetic current density
j_0 (A cm^{-2})	exchange current density
j_f (A cm^{-2})	kinetic current for forward reaction
j_L (A cm^{-2})	mass-transport limiting current density
k (meV K^{-1})	Boltzmann constant, 0.08617
ki, k-i (s^{-1} or cm^3 mol^{-1}s^{-1})	rate constants of elementary reactions, i = DA, OA, OD
T (K)	temperature
ϵ (eV)	coverage-dependent free energy of adsorption
γ	adsorption range constant
λ	coefficient for adsorption on activation free energy
η (V)	HOR overpotential
σ_{DA}, σ_{OA}, σ_{OD}	symmetry factor for the effect of adsorption energy
θ	fractional coverage of the reaction intermediate
θ^0	equilibrium coverage, θ at $\eta = 0$
ν_{DA}, ν_{OA}, ν_{OD} (mol s^{-1} cm^{-2})	reaction rates of the elementary steps

ΔG_{ad}^{0} (eV)	adsorption free energy for $^1/_2H_2 \rightarrow H_{ad}$ at $\eta = 0$
ΔG_{DA}^{*0}, ΔG_{OA}^{*0}, ΔG_{OD}^{*0} (eV)	activation free energy at $\eta = 0$
$\Delta G_{DA}^{*0'}$, $\Delta G_{OA}^{*0'}$(eV)	activation free energy at $\eta = 0$ and $\Delta G_{ad}^{0} = 0$

Supporting Information Available: Kinetic analysis using the model with coverage-dependent lateral repulsion. This material is available free of charge via the Internet at http://pubs.acs.org.

References and Notes

(1) Breiter, M. W. Reaction mechanisms of the H2 oxidation/evolution reaction. In *Handbook of Fuel Cells*; Vielstich, W., Lamm, A., Gasteiger, H. A., Eds.; Wiley: New York, 2003; Vol. 2 Electrocatalysis, Chapter 25, p 361.

(2) Markovic, N. M. The hydrogen electrode reaction and the electrooxidation of CO and H2/CO mixtures on well-characterized Pt and Pt-bimetallic surfaces. In *Handbook of Fuel Cells*; Vielstich, W., Lamm, A., Gasteiger, H. A., Eds.; Wiley: New York, 2003; Vol. 2 Electrocatalysis, Chapter 26, p 368.

(3) Gattre, M.; MacDougall, B. Reaction mechanisms of the O2 reduction/evolution reaction. In *Handbook of Fuel Cells*; Vielstich, W., Lamm, A., Gasteiger, H. A., Eds.; Wiley: New York, 2003; Vol. 2 Electrocatalysis, Chapter 30, p 443.

(4) Bockris, J. O. M. Electrode Kinetics. In *Modern Aspects of Electrochemistry*; Bockris, J. O. M., Ed.; Scientific Publications: London, 1954; Chapter 4, p 180.

(5) Vetter, K. J. *Electrochemische Kinetik*; Springer-Verlag: Berlin, 1961.

(6) Conway, B. E.; Tilak, B. V. *Electrochim. Acta* **2002**, *47*, 3571.

(7) Chen, A.; Kucernak, A. *J. Phys. Chem. B* **2004**, *108*, 13984.

(8) Gasteiger, H. A.; Markovic, N. M.; Ross, P. N. *J. Phys. Chem.* **1995**, *99*, 8290.

(9) Wang, J. X.; Springer, T. E.; Adzic, R. R. *J. Electrochem. Soc.* **2006**, *153*, A1732.

(10) Jerkiewicz, G. *Prog. Surf. Sci.* **1998**, *57*, 137.

(11) Conway, B. E.; Jerkiewicz, G. *Electrochim. Acta* **2000**, *45*, 4075.

(12) Kunimatsu, K.; Uchida, H.; Osawa, M.; Watanabe, M. *J. Electroanal. Chem.* **2006**, *587*, 299.

(13) Nichols, R. J.; Bewick, A. *J. Electroanal. Chem.* **1988**, *243*, 445.

(14) Nichols, R. J. *IR Hopd*; VCH: New York, 1992.

(15) Protopopoff, E.; Marcus, P. *J. Electrochem. Soc.* **1988**, *135*, 3073.

(16) Trasatti, S. Adsorption−Volcano curve. In *Handbook of Fuel Cells*; Vielstich, W., Lamm, A., Gasteiger, H. A., Eds.; Wiley: New York, 2003; Vol. 2 Electrocatalysis, Chapter 10, p 88.

(17) Schmickler, W.; Trasatti, S. *J. Electrochem. Soc.* **2006**, *153*, L31.

(18) Parsons, R. *Trans. Faraday Soc.* **1958**, *54*, 1053.

(19) Nørskov, J. K.; Bligaard, T.; Logadottir, A.; Kitchin, J. R.; Chen, J. G.; Pandelov, S. *J. Electrochem. Soc.* **2005**, *152*, J23.

(20) Nørskov, J. K.; Bligaard, T.; Logadottir, A.; Kitchin, J. R.; Chen, J. G.; Pandelov, S.; Stimming, U. *J. Electrochem. Soc.* **2006**, *153*, L33.

(21) Greeley, J.; Jaramillo, T. F.; Bonde, J.; Chorkendorff, I.; Norskov, J. K. *Nat. Mater.* **2006**, *5*, 909.

(22) Tafel, J. *Z. Phys. Chem., Stoechim. Verwandtschaftsl.* **1905**, *50*, 641.

(23) Heyrovsky, J. *Recl. Trav. Chim. Pays-Bas* **1927**, *46*, 582.

(24) Volmer, T.; Erdey-Gruz, M. *Z. Phys. Chem. Abt. A* **1930**, *150*, 203.

(25) Norskov, J. K.; Bligaard, T.; Logadottir, A.; Kitchin, J. R.; Chen, J. G.; Pandelov, S. *J. Electrochem. Soc.* **2005**, *152*, J23.

(26) Quaino, P. M.; Fernandez, J. L.; de Chialvo, M. R. G.; Chialvo, A. C. *J. Mol. Catal. A* **2006**, *252*, 156.

(27) Cai, Y.; Anderson, A. B. *J. Phys. Chem. B* **2004**, *108*, 9829.

(28) The DFT calculations within the DMol3 code used the generalized gradient approximation with the spin-restricted PW91 functional. The Kohn-Sham one-electron equations were solved on a basic set of double numerical plus d functions (comparable to a Gaussian 6−31G(d)) with kinetic energies below 5.0 Å, and semi-core pseudo-potentials described the ionic cores. The Pt(111) surface was modeled by a four-layer slab, separated by an 11 Å thick vacuum. H adsorptions on a bare Pt(111) and the H pre-adsorbed Pt(111) were included in a 2′1 super-cell. In all cases, H and the first two Pt layers were allowed to relax, while the Pt atoms in the bottom two layers were fixed at the substrate's lattice position. The differential adsorption energy of H on Pt(111) was expressed as $\Delta E_H = E[(i + 1)H/Pt(111)] - 1/2E(H_2) - E[iH/Pt(111)]$, where "*i*" is the number of H atoms pre-adsorbed per unit cell. In addition, for each optimized structure, a Mulliken population analysis was carried out to estimate the partial charge on each atom and examine qualitative trends in charge redistribution.

(29) Markovic, N. M.; Grgur, B. N.; Ross, P. N. *J. Phys. Chem. B* **1997**, *101*, 5405.

(30) Zolfaghari, A.; Jerkiewicz, G. *J. Electroanal. Chem.* **1999**, *467*, 177.

(31) Adzic, R. R.; Feddrix, F.; Nikolic, B. Z.; Yeager, E. *J. Electroanal. Chem.* **1992**, *341*, 287.

(32) Watson, G. W.; Wells, R. P. K.; Willock, D. J.; Hutchings, G. J. *Chem. Commun.* **2000**, *2000*, 705.

(33) Ford, D. C.; Xu, Y.; Mavrikakis, M. *Surf. Sci.* **2005**, *587*, 159.

(34) Ishikawa, Y.; Mateo, J. J.; Tryk, D. A.; Cabrera, C. R. *J. Electroanal. Chem.* in press.

(35) Norskov, J. K.; Rossmeisl, J.; Logadottir, A.; Lindqvist, L.; Kitchin, J. R.; Bligaard, T.; Jonsson, H. *J. Phys. Chem. B* **2004**, *108*, 17886.

(36) Shao, M. H.; Adzic, R. R. *Electrochim. Acta* **2005**, *50*, 2415.

(37) Gerischer, H. *Z. Phys. Chem. N. F.* **1956**, *8*, 137.

(38) Trasatti, S. *J. Electroanal. Chem.* **1972**, *39*, 163.

(39) Sabatier, P. *Ber. Dtsch. Chem. Ges.* **1911**, *44*, 1984.